GlobalNav: Daily Object Navigation in VLM-based Autonomous Mobile Systems with Aligned Local and Global Views

ABSTRACT

Autonomous mobile systems are increasingly deployed to provide location-based services, such as guided tour and retrieving objects. However, current navigation paradigms rely almost exclusively on onboard egocentric perception. Because real-world items are highly dynamic and placed in unpredictable locations, these systems frequently degrade into inefficient, exhaustive searches. While indoor environments (e.g., elderly homes and offices) are densely equipped with infrastructure cameras (e.g., CCTV) that provide a continuous global view, bridging the severe perspective gap between elevated infrastructure nodes and low-angle autonomous systems remains a non-trivial systems challenge. To address this, we present GlobalNav, a new infrastructure-assisted VLM-based navigation system that integrates global infrastructure camera views with local autonomous system perception through semantic-guided cross-view alignment. To enable reliable cross-node collaboration, GlobalNav introduces a discretized spatial topology and a cross-view perspective alignment module that fuses visual, semantic, and spatial features, effectively aligning heterogeneous viewpoints without requiring precise 3D maps. Furthermore, to handle local occlusions and dynamic obstacles invisible to the infrastructure, we design a hierarchical navigation strategy that uses globally identified landmarks as high-level targets, falling back to local waypoints when global guidance cannot be directly followed. Extensive evaluations on both real-world robotic testbeds and high-fidelity simulations demonstrate that GlobalNav significantly improves upon state-of-the-art baselines, increasing navigation success rates by nearly 40% and reducing average searching path lengths by 20%.

1 INTRODUCTION

Empowered by recent advancements in Vision-Language Models (VLMs), autonomous mobile systems are increasingly deployed to provide intuitive location-based services. The adoption of these systems has surged by over 30% worldwide [8]. For example, the autonomous system can help users to grab the dishes in a restaurant and take the glasses at home. Users expect these systems to interpret natural language queries and navigate to targets in environments with items ranging from large static furniture to highly mobile personal items.

However, current mobile navigation paradigms rely almost exclusively on egocentric (onboard) perception. Existing Object-Goal Navigation [5, 13] and Vision-Language

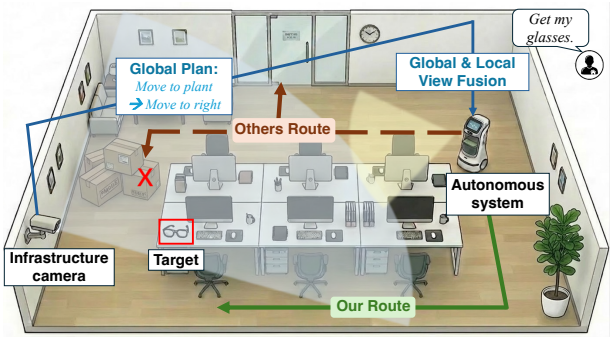

Figure 1: Daily object navigation in VLM-based autonomous mobile systems.

Navigation methods [1, 33] either depend on pre-built static maps, which immediately become obsolete when daily objects are moved, or rely on VLM-driven commonsense priors to guess an object's location. Because personal items are placed in unpredictable locations that defy typical semantic expectations, these egocentric approaches frequently degrade into exhaustive, blind searches. Consequently, state-of-the-art methods remain severely limited, with success rates below 30% for daily object localization.

To overcome the fundamental visibility limitations of VLM-based mobile autonomous systems, we look toward the surrounding infrastructure cameras that have already been densely deployed in environments, such as surveillance camera systems in elderly homes and public CCTV networks in offices and restaurants. These cameras provide a continuous, elevated global view of the environment. As illustrated in Figure 1, we aim to leverage the local and global views from the autonomous mobile system and the smart infrastructure to enable semantically-based navigation that can be readily fit with the existing VLM-based mobile autonomous systems.

However, enabling this infrastructure-assisted autonomous mobile navigation paradigm introduces a formidable systems challenge: bridging the severe perspective gap between distributed, heterogeneous viewpoints. The infrastructure camera's elevated, wide-angle global view is drastically inconsistent with the mobile system's low-angle, egocentric local view. Direct geometric projection or naive image-matching between these nodes fails due to partial observability, depth estimation errors inherent in monocular infrastructure cameras, and dynamic occlusions. Furthermore, the global view provides only a high-level layout and lacks ground-level detail, meaning planned routes may be locally unreachable due to unseen obstacles, and the autonomous system may move

out of the infrastructure camera's line of sight, preventing continuous visual tracking and navigation update.

To address these challenges, we propose *GlobalNav*, a novel infrastructure-assisted mobile navigation system that semantically aligns global infrastructure views with local mobile perception. As shown in Figure 2, GlobalNav first provides navigation instructions given as a series of landmarks in the global view. Meanwhile, it leverages VLMs to construct a discretized, topological spatial representation shared across both nodes. We introduce a cross-view perspective alignment module that fuses visual, semantic, and spatial features to reliably associate shared landmarks and estimate perspective transformations across the network. Building on this distributed alignment, GlobalNav employs a fault-tolerant, hierarchical navigation protocol: the infrastructure provides high-level, VLM-reasoned landmark chains, while the autonomous system dynamically falls back to local, Voronoi-based waypoint selection to bypass unforeseen occlusions and maintain continuous progress.

Our proposed system offers several advantages over existing navigation paradigms. First, GlobalNav eliminates the need for prior exploration or pre-built maps to ensure its robustness to dynamic environmental changes. Second, it bridges the severe perspective gap between the elevated infrastructure camera and the mobile system's low-angle view through robust cross-view landmark alignment to provide continuous guidance even within blind spots. Finally, GlobalNav can leverage deterministic visual evidence from the global viewpoint, effectively overcoming visibility limitations to reliably retrieve small, arbitrarily placed daily items.

The core contributions of GlobalNav are:

- We design discretized spatial topology module to construct structured scene representation of both global and local views. By discretizing continuous spatial relationships, this approach is highly resilient to the depth estimation errors inherent in monocular infrastructure cameras, and is explicitly designed to be easily interpreted by the VLM for the subsequent hierarchical navigation strategy.
- We develop a cross-view perspective alignment mechanism that bridges the perspective gap between the elevated infrastructure camera and the autonomous system's low-angle view, enabling accurate localization and continuous navigation guidance even when the autonomous system enters the camera's blind spots.
- We introduce a hierarchical navigation framework that bridges global infrastructure guidance with local egocentric execution. By employing VLM-reasoned landmark chains for high-level path planning and dynamically falling back to Voronoi-based local waypoint selection to bypass unforeseen occlusions, our system provides a fault-tolerant mechanism that ensures continuous and reliable navigation toward arbitrarily placed daily objects.

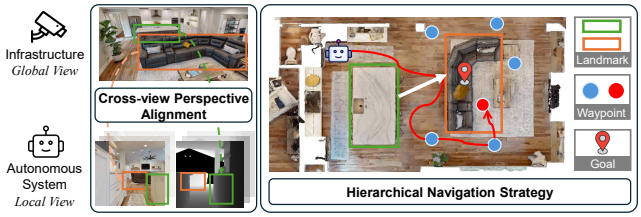

Figure 2: GlobalNav for daily object navigation.

We extensively evaluate GlobalNav in both simulated environments in the Habitat simulator [16] and on a real-world autonomous system in environments (e.g., restaurants, homes, and offices). Experiment results show that GlobalNav significantly outperforms state-of-the-art baselines, achieving nearly 40% improvement in navigation success rate while reducing average path length by 20%. Moreover, GlobalNav reduces VLM token consumption and search time by 40% and 50%, respectively, compared to existing VLM-based methods, demonstrating that GlobalNav achieves robust and efficient navigation with significantly reduced search overhead.

2 MOTIVATIONAL STUDY

In this section, we present a motivational case study to illustrate the limitations of traditional navigation methods. First, we demonstrate the disadvantages of relying solely on an autonomous system's egocentric perception and commonsense priors in navigation, thereby highlighting the necessity of introducing the infrastructure camera's global view to enable fast and efficient navigation. Furthermore, we also show the limitations of existing navigation methods when naively incorporating global views as a reference, i.e., directly feeding the global view to VLM.

2.1 Egocentric Object-Goal Navigation

To understand the limitations of current object-goal navigation methods which solely rely on the autonomous system's local egocentric view and commonsense priors, we conduct a motivational experiment of navigating to randomly placed daily items. We use the Habitat Simulator [16] with scenes from the HM3D dataset [17] to evaluate three SOTA methods, i.e., Frontier [29], InstructNav [12], and SG-Nav [27], over daily objects such as backpack, laptop, and glasses.

Figure 3a shows the navigation paths produced by these methods, all of which fail to produce targeted paths to the objects. Instead, these paths exhibit high redundancy that spans large portions of the environment without converging on the target. We also demonstrate their success rate and search time in Figure 3b and Figure 3c. Without access to real-time scene information, these methods cannot reliably reason about the target's location, making the autonomous systems to resort to exhaustive environmental coverage that degrades search efficiency and can result in navigation failure.

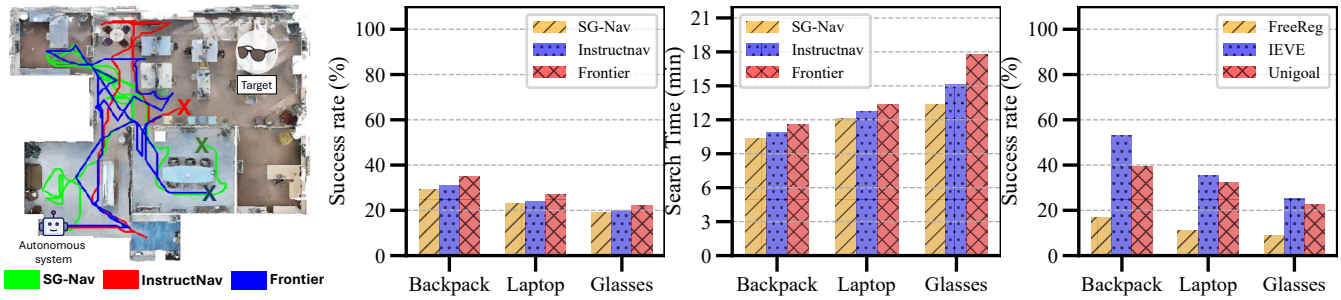

(a) Trajectories (egocentric) **(b) Success rate (egocentric)** **(c) Search time (egocentric)** **(d) Success rate (reference view)**

Figure 3: A motivational study on existing navigation methods. a) - c) show results from egocentric navigation methods. d) shows the result from navigation with reference view.

These results expose two critical limitations of these existing methods. First, commonsense-driven methods are ill-suited for locating movable daily items. While such methods succeed on semantically predictable targets (e,g., a pillow is on a bed), they can easily fail on objects like glasses, which can be arbitrarily placed on any surface or be blocked. As evidenced by the winding trajectories in Figure 3a, when commonsense priors cannot provide reliable spatial guidance, the navigation degenerates into blind search. Second, unlike large furniture in the room, small objects are difficult to detect from the autonomous system which usually stands at a low viewpoint. Navigation to small daily items usually requires the mobile system to navigate into close proximity and achieve an unoccluded line of sight. These limitations demonstrate that heuristic-driven, egocentric navigation methods are ill-equipped for daily object retrieval.

2.2 Navigation with the Global View as Reference

We measure the performance of naively adapting existing approaches to incorporate a global infrastructure view for navigation. We evaluate three methods in Habitat using real-world scenes: (1) a map-based method FreeReg [22], which constructs a 3D map of the scene and we project the infrastructure image onto it to localize the target object; (2) an instance image-goal navigation method IEVE [11] that originally uses an object image as a reference to guide cross-view matching, where we naively substitute the global infrastructure view as the reference image to identify correspondences with the target object's local appearance; (3) a VLM-based method UniGoal [28] which originally encodes a target object alongside its surrounding semantic context from a local reference image into a rich embedding to guide navigation, and we naively substitute the global infrastructure view as the reference input for the same pipeline.

As shown in Figure 3d, FreeReg only achieves a success rate below 20%. This is because the severe viewpoint disparity between the infrastructure camera's view and the SLAM map renders unreliable cross-view feature matching. IEVE degrades sharply as object size decreases, since smaller objects yield fewer distinguishable feature points, significantly reducing the accuracy of image matching. Unigoal similarly yields limited success, as the global infrastructure view contains rich semantic and spatial information, including overall room layout, inter-object relationships, and long-range navigational structure, which cannot be fully reasoned by naively feeding the image into the VLM. Without a structured decomposition of this visual content, the VLM fails to extract and ground the spatial context necessary for object navigation, leading to inefficient trajectories and frequent failure.

3 SYSTEM DESIGN

Given a natural language query such as "grab me a yellow backpack", GlobalNav utilizes an infrastructure camera, such as a home surveillance or CCTV camera, to extract rich spatial and semantic features from the global perspective and guide the autonomous system's navigation. Correspondingly, we assume that the autonomous mobile system is equipped with a standard RGB-D camera to find and navigate toward the target object based on the navigation guides.

GlobalNav is designed following three key principles. First, it does not require the autonomous system to remain visible to the infrastructure camera, and can still infer its location and provide navigation guidance even in a blind spot of the infrastructure's view. Second, it achieves robust cross-view understanding to enable the autonomous system to accurately follow the infrastructure's guidance despite the significant viewpoint discrepancy between the two views. Third, it features an adaptive navigation strategy that treats the globally planned path as high-level guidance, allowing the autonomous system to dynamically adapt when the global plan conflicts with locally observed conditions.

3.1 System overview

Figure 4 shows the overview of GlobalNav. When the user submits a query, the system forwards it to the edge server, which captures the current global view from the infrastructure camera and processes it on demand. Both the edge server

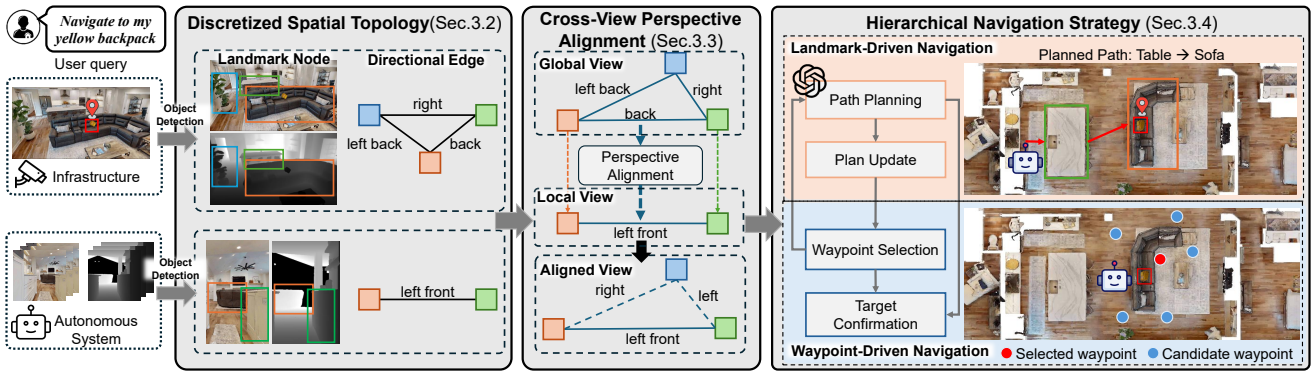

Figure 4: System architecture of GlobalNav

and the autonomous system independently detect landmarks and extract semantic and spatial features from their respective views (Section 3.2). The edge server then queries the VLM to identify the most related landmark to the target object and establish a spatial relationship between them (e.g., *"the <backpack> is located to the right of the <sofa>"*), which provides fine-grained contextual guidance for the final retrieval stage. The autonomous system transmits its locally extracted features to the edge server, which performs cross-view matching to align landmarks observed in the local view with those in the global view, estimating the perspective transformation between the two viewpoints (Section 3.3). With this correspondence established, the edge server sends navigation guidance to the autonomous system, which begins navigating toward the target object under a hierarchical navigation strategy operating at two levels (Section 3.4). At the high level, the infrastructure plans a chain of landmarks via the VLM on cloud for the autonomous system to follow and updates this chain when obstructions are detected. At the low level, when the edge server is unable to identify new landmarks to update the chain, the autonomous system switches to local waypoint-driven navigation to bypass obstacles while keeping on track toward the next landmark. When the autonomous system reaches the target landmark, it also selects local waypoints to comprehensively search the surrounding area to locate the target object. Note that GlobalNav assumes the autonomous system can exchange textual messages with the edge server using existing wireless infrastructure, e.g., Wi-Fi or the Internet.

3.2 Discretized Spatial Topology

As the first step of the system, both the infrastructure camera and the autonomous system independently construct a structured scene representation from their respective views, which serves as the shared foundation for cross-view perspective alignment and navigation reasoning. Reliable cross-view matching and navigation guidance depend on a shared structural representation of the scene that is consistent across both the infrastructure's global view and the autonomous system's local view. As shown in Figure 4, we represent the scene as a topological graph, where each node corresponds to a detected landmark enriched with semantic features, and each directed edge encodes the discretized relative direction between a pair of landmarks.

3.2.1 Landmark Node Construction. For both the infrastructure image I^{infra} and the autonomous system's egocentric RGB stream, we apply a detection model to detect and localize navigational landmarks, denoted as $[I_1^{infra}, I_2^{infra}, \dots]$ and $[I_1^{auto}, I_2^{auto}, \dots]$ respectively. We then query the VLM to generate a fine-grained textual description for each detected landmark, such as "brown L-shaped sofa", yielding description sets $[T_1^{infra}, T_2^{infra}, \dots]$ and $[T_1^{auto}, T_2^{auto}, \dots]$ for the infrastructure and the autonomous system, respectively.

3.2.2 Directional Edge Construction. Spatial relationships between landmarks are essential for the VLM-based path planning and navigation reasoning in subsequent stages, as they provide the structural context needed to interpret the scene layout and generate meaningful navigation guidance. However, determining spatial relationships between landmarks requires accurate 3D coordinates, which are difficult to obtain from the infrastructure camera since it captures only 2D images. Without precise absolute coordinates, we discretize spatial relationships into eight directional categories (*front, front-left, left, back-left, back, back-right, right, front-right*), which provides a consistent spatial representation across both views. To obtain these relationships, the infrastructure employs a monocular depth estimation method [3] to get relative 3D positions from its 2D image, directly obtains 3D landmark positions from its onboard depth camera. Let $\mathbf{c}_i = (x_i, y_i, z_i)$ and $\mathbf{c}_j = (x_j, y_j, z_j)$ denote the 3D centroids of landmarks i and j; by projecting onto the horizontal ground plane, the relative deviation angle is computed as $\theta_{i,j} = \text{atan2}(y_j - y_i, x_j - x_i)$, where $\theta_{i,j} \in [-\pi, \pi]$. These angles are then mapped into eight uniform directional bins, each spanning $\frac{\pi}{4}$ radians, yielding the pairwise directional

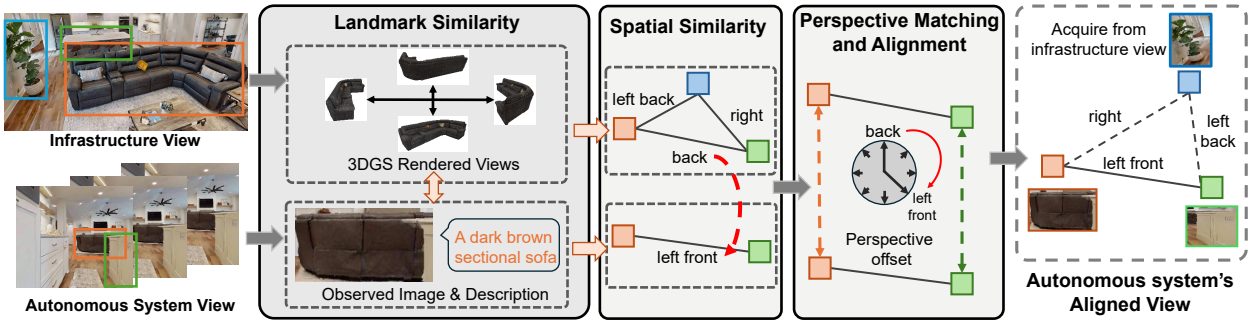

Figure 5: The Cross-View Perspective Alignment Module.

edge matrices E^{infra} and E^{auto} for the infrastructure and autonomous system views, respectively. In particular, to ensure directional labels are consistent with how a VLM interprets spatial relationships, we define a canonical coordinate system for VLM reasoning over the infrastructure image, where the horizontal axis corresponds to *left–right* and depth relative to the camera defines *front–back*. This allows the VLM to directly leverage these directional labels when locating landmarks and selecting navigation waypoints.

3.3 Cross-View Perspective Alignment

Given the topological graphs constructed from both views, the mobile system need to establish landmark correspondences across the two views and estimates the directional offset between their spatial reference frames, which is essential for navigation. Landmark correspondences ensure that the two sides reason about the same physical entities, and directional alignment resolves the spatial discrepancies across views (e.g., a table to the right of a sofa from the mobile system's view may appear to the left in the infrastructure's view), so that navigation instructions can be correctly interpreted. However, severe viewpoint discrepancies and partial observability make traditional geometry-based localization methods [22, 4] prone to failure in such settings. As shown in Figure 5, we propose a cross-view perspective alignment algorithm that jointly leverages categorical, visual, and semantic landmark similarities with pairwise directional consistency to simultaneously recover landmark correspondences and estimate the directional offset, providing the VLM with a unified spatial representation for navigation reasoning.

3.3.1 Landmark Node Similarity. To establish accurate correspondences between landmarks detected by the infrastructure and the autonomous system, we compute a robust similarity score for each landmark pair. Direct comparison of 2D image crops is unreliable due to partial occlusion and severe viewpoint discrepancies. Instead, we obtain the infrastructure's 3D scene representation via Gaussian Splatting [20] to reconstruct each infrastructure landmark i and render V views at equal angular intervals, yielding a comprehensive visual profile $[\hat{I}^{infra}_{i,1}, \ldots, \hat{I}^{infra}_{i,V}]$. To compute the similarity for each landmark pair (i, j), we first apply a categorical gate $S^{class}_{i,j} = \mathbf{1}[C^{infra}_i = C^{auto}_j]$ to immediately discard class-mismatched pairs. For the remaining pairs, we compute two similarity scores using an image encoder Φ_{img} and a text encoder Φ_{text}. The visual similarity $S^{visual}_{i,j} = \frac{1}{V}\sum_v \Phi_{img}(I^{auto}_j) \cdot \Phi_{img}(\hat{I}^{infra}_{i,v})$ measures appearance consistency by comparing the autonomous system's landmark image against the rendered representation from infrastructure's view. The cross-modal semantic similarity $S^{semantic}_{i,j} = \frac{1}{V}\sum_v \Phi_{text}(T^{auto}_j) \cdot \Phi_{img}(\hat{I}^{infra}_{i,v})$ further evaluate the match by aligning the landmark's textual description against the rendered views. The overall landmark node similarity is:

$$S^{landmark}_{i,j} = S^{class}_{i,j}\left(\alpha_1 \cdot S^{visual}_{i,j} + \alpha_2 \cdot S^{semantic}_{i,j}\right). \quad (1)$$

Only pairs exceeding threshold τ are retained as candidate landmark correspondences C to reduce the search space for the subsequent graph matching.

3.3.2 Directional Edge Similarity. Besides individual landmark similarity, we also compute directional edge similarity between landmark pairs in the infrastructure's and mobile system's views. Given the eight-directional spatial edges $e^{infra}_{i,j}$ and $e^{auto}_{m,n}$ between landmark pairs in the infrastructure and autonomous system graphs respectively, we define a smooth cosine-based directional similarity to account for slight deviations caused by perspective differences or occlusions (e.g., a "front-left" relationship being perceived as purely "left"):

$$S^{dir}(e^{infra}_{i,j}, e^{auto}_{m,n}) = \frac{1}{2}\left[1 + \cos\left(\frac{2\pi}{8}\left(e^{infra}_{i,j} - e^{auto}_{m,n}\right)\right)\right]. \quad (2)$$

This function assigns a score of 1 for an exact directional match, a moderate score for adjacent directions, and 0 for completely opposite directions. Spatial edge similarity is evaluated only for edges connecting pairs within C, avoiding redundant computation.

3.3.3 Perspective Matching and Alignment. With both landmark node and directional edge similarities defined, we now jointly estimate landmark correspondences and the perspective transformation between the two views. Because spatial directions are discretized into eight bins, the perspective transformation reduces to a single discrete rotational offset $k \in \{0, 1, \ldots, 7\}$, where each increment corresponds to a rotation of $\frac{\pi}{4}$ radians. Applying offset k to the infrastructure direction yields $\hat{e}_{i,j}^{infra}(k) = (e_{i,j}^{infra} + k) \pmod 8$. For each candidate offset k, we perform spectral graph matching [7] by constructing an affinity matrix $\mathbf{M}(k)$ over the candidate set C, where each row and column is indexed by a pair $(i, m) \in C$. The diagonal entries store per-node appearance similarities $S_{i,m}^{landmark}$. Each off-diagonal entry between two distinct candidate pairs (i, m) and (j, n) captures the pairwise edge consistency $S^{dir}(\hat{e}_{i,j}^{infra}(k), e_{m,n}^{auto})$ under the current rotational offset, with all other entries set to zero. The principal eigenvector $\mathbf{x}^*(k)$ of $\mathbf{M}(k)$ then yields the confidence of each candidate correspondence, and the optimal offset is selected as:

$$k^* = \arg\max_{k \in \{0,\ldots,7\}} \mathbf{x}^*(k)^\top \mathbf{M}(k)\, \mathbf{x}^*(k). \tag{3}$$

Together, the matched landmark pairs $\mathcal{P}$ and the optimal perspective offset k^* provide the VLM with a unified spatial reference frame for the subsequent navigation.

3.4 Hierarchical Navigation Strategy

With landmark correspondences and perspective transformation established, the system uses this aligned spatial context to guide the autonomous system toward the target object. While the infrastructure can plan a global navigation route as a chain of landmarks, such a route is not always locally executable as the autonomous system may encounter obstacles invisible from the global view or fail to observe expected landmarks due to local occlusions. To address this, we propose a Hierarchical Navigation Strategy operating at the landmark level and the waypoint level. Figure 6 shows the pipeline of this module. The system operates primarily at the landmark level: *Path Planning* generates an ordered sequence of landmarks toward the target for the autonomous system to follow, and *Path Update* reroutes through an alternative landmark if the next one becomes unreachable. When no alternative landmarks can be identified, the system falls back to the waypoint level, where *Waypoint Selection* identifies a local navigable waypoint to bypass the obstruction and reacquire the next landmark. Upon reaching the final landmark, *Target Confirmation* selects the waypoint most likely to bring the target object into view.

3.4.1 Landmark-Driven Navigation. The landmark-level navigation combines two complementary mechanisms: *Path Planning* generates an ordered landmark chain toward the target, and *Path Update* reroutes through alternative landmarks when the planned path is obstructed. If the autonomous system initially fails to match any landmarks to the infrastructure view, it first constructs a panoramic image from its observations and prompts a VLM to infer the most promising direction toward the infrastructure's observable region.

Path Planning. This stage is activated when the autonomous system successfully matches one or more of its observed landmarks with those in the infrastructure view. Given the infrastructure image, the target object, and the currently matched landmarks, the VLM performs Chain-of-Thought (CoT) reasoning to generate an ordered chain of landmarks as the navigation route, starting from a currently visible landmark and ensuring that each subsequent landmark is observable from the preceding one. The autonomous system then follows this chain sequentially, denoted as $[L_1, L_2, ...]$, proceeding to the next landmark upon reaching the current one.

Path Update. This stage is triggered when the autonomous system reaches L_{current} but fails to visually locate or navigate to L_{next}, typically due to occlusion. Given the autonomous system's current observations and the infrastructure landmark layout, the VLM selects an alternative intermediate landmark to bypass the obstruction and reacquire L_{next}.

3.4.2 Waypoint-Driven Navigation. When landmark-level navigation is insufficient either because the next landmark cannot be located or because the autonomous system has reached the terminal landmark and must search for the target object, the system falls back to fine-grained waypoint-driven navigation. Both stages below share a common mechanism: we extract the autonomous system's currently observable navigable region and discretize it using a Reduced Voronoi graph [24], where nodes represent navigable waypoints and edges denote their connectivity. To enable VLM-based reasoning over these waypoints, each node is assigned a structured spatial description relative to nearby landmarks within a 1.5-meter radius. For each node-landmark pair, we identify the closest point on the landmark's surface, compute the directional vector from the node to that point, and quantize it into one of eight discrete directions. A cross-view transformation is then applied to convert egocentric directions into the infrastructure's coordinate frame. Combined with the metric distance, this yields a textual description per node formatted as: *"This node is to the <direction> of <landmark>, at a distance of <distance>."*

Waypoint Selection. This stage is triggered when the autonomous system reaches L_{current} but can neither locate L_{next} nor identify any alternative landmark to navigate toward. We filter the Voronoi nodes to retain only those referencing L_{current}, and prompt the VLM with these candidates alongside the global relative direction from L_{current} to L_{next}. The

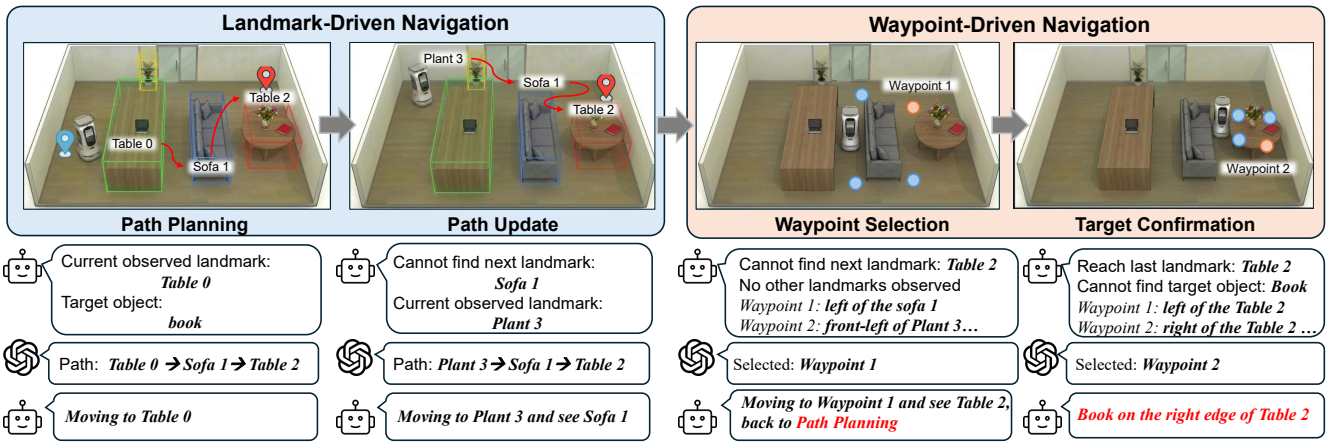

Figure 6: Illustration of Hierarchical Navigation Strategy.

VLM selects a waypoint that aligns with the target direction while remaining proximal to L_{current}, effectively guiding the autonomous system around the occlusion to reestablish visual contact with L_{next}.

Target Confirmation. This stage is activated upon reaching the terminal landmark. Since the target object may remain undetected due to its small size or occlusion by the landmark itself, we use the waypoints from Voronoi graph around the terminal landmark and retrieve the spatial relationship between the target and the landmark established in Section 3.2 (e.g., *"the cellphone is on the far left edge of the table"*). The VLM then selects the viewing position most likely to bring the target object into view.

3.4.3 Fault-Tolerant Recovery. To guard against perceptual errors from cross-view discrepancies, GlobalNav incorporates a two-level recovery mechanism. At the landmark navigation level, if the landmark matching relationship changes during transit (i.e., indicating a corrected perceptual mismatch), the autonomous system immediately aborts the current path and reverts to *Path Planning* to compute a revised navigation chain. At the waypoint navigation level, if all candidate Voronoi nodes are exhausted during *Waypoint Selection* without reacquiring L_{next}, or if the target object cannot be located during *Target Confirmation*, the system treats the outcome as a false positive match or a navigational dead end. In either case, the offending landmark is invalidated and replanning is triggered to find an alternative route, preventing localized failures from cascading.

4 TESTBED AND DATASET

Existing robot navigation datasets predominantly focus on egocentric perception and lack the inclusion of infrastructure or global viewpoints. Therefore, to rigorously evaluate GlobalNav, we establish a comprehensive testbed encompassing a novel dataset constructed in the Habitat simulator and real-world robotic deployments. The details of our experimental testbed and dataset generation are outlined below.

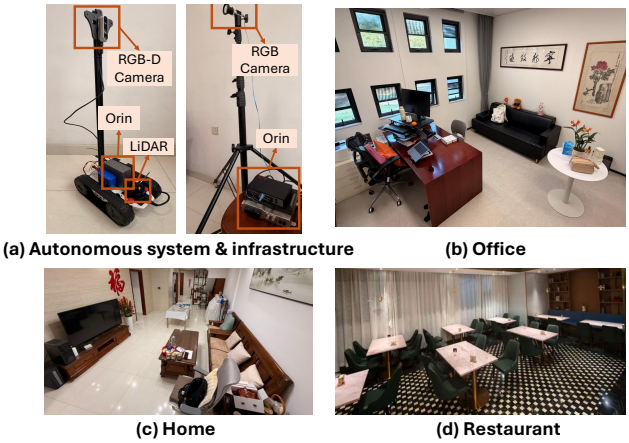

Figure 7: Real-world experiment setup and scenes.

4.1 Real-world Setup

To validate GlobalNav in a real-world setting, we deploy our system on a physical testbed as illustrated in Figure 7. The autonomous system is built on an Agile LIMO robot chassis equipped with an Intel RealSense D435i RGB-D camera (640× 480) for egocentric perception and a RoboSense Airy LiDAR for visual odometry, providing real-time position and pose estimates relative to the starting point. The infrastructure side consists of a portable elevated platform mounted with a Basler RGB camera (1200 × 1920), with both sides using NVIDIA Jetson Orin and communicating over an indoor 802.11ac Wi-Fi network. We evaluate across 10 real-world scenes including home, office, and restaurant environments. Each episode requires the autonomous system to locate a personal daily object such as a backpack, mug, or glasses, with 300 episodes in total. Optimal navigation paths are

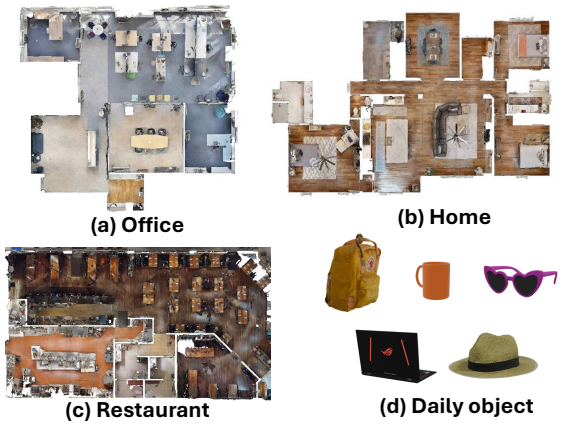

Figure 8: Habitat simulator experiment scenes.

Dataset	#scenes	#infrastructure	#episodes	#coverages
Real-world	10	30	300	30-110 m^2
Habitat	20	80	1500	40-90 m^2

Table 1: Summary of datasets in the simulator and real-world.

obtained via Polycam [15] 3D scene reconstruction and serve as the reference for path efficiency evaluation

4.2 Habitat Simulator Setup

We conduct simulated experiments using the Habitat simulator [16], a widely adopted platform for embodied AI and robotic navigation research. Our evaluation environments are drawn from the Habitat-Matterport 3D (HM3D) dataset [17], which provides high-fidelity, photorealistic 3D scans of diverse real-world indoor spaces. We select 20 distinct scenes spanning a range of functional area types, including homes, offices, and restaurants. To simulate our proposed infrastructure-assisted navigation paradigm, we strategically place 3 to 5 virtual infrastructure cameras within each scene to provide elevated, global viewpoints of varying coverage. To ensure robust evaluation across varying degrees of navigational difficulty, we define 3 to 5 distinct starting positions for the autonomous system in each scene. For navigation targets, we integrate five 3D object models sourced from the PIN dataset [2], including a backpack, mug, eyeglasses, laptop, and hat, representing everyday items of diverse appearance. To reflect the spatial unpredictability inherent in real-world scenarios, each object is dynamically placed at 2 to 5 different locations within each environment. The autonomous system is equipped with an RGB-D camera at a resolution of 480×640, while each infrastructure camera is configured at 720×1280. To evaluate performance across environments of varying difficulty, we quantify scene complexity using the Voronoi diagram [24, 9] of each environment's navigable space, where nodes represent waypoints and edges denote navigable connectivity. We adopt the element complexity metric from [26], defined as the total number of nodes and edges, where a higher count reflects greater spatial complexity and navigational difficulty. Our selected scenes span a wide range of complexities, enabling a comprehensive assessment of system robustness under both simple and challenging environments.

5 EVALUATION

5.1 Implementation

For all VLM queries, we use GPT-5.2. Landmark detection in both the infrastructure and autonomous system views is performed using Grounding SAM [18], while depth estimation for the infrastructure view relies on DepthPro [3]. Holistic 3D representations of landmarks are obtained via SAM-3D [20], and appearance and description features for landmark matching and perspective alignment are extracted using the image and text encoders from FG-CLIP [25]. A maximum step limit of 500 is imposed; navigation episodes in which the autonomous system fails to locate the target within this budget are marked as failures. Simulated experiments are conducted on a PC equipped with an AMD 5950X CPU and an NVIDIA RTX 4090 GPU, while real-world experiments follow the testbed setup described in Section 4.1.

5.2 Evaluation and Baselines

5.2.1 Metrics. To comprehensively evaluate the performance and efficiency of our proposed navigation framework, we adopt several standard metrics widely used in embodied AI and object-goal navigation research. Success Rate (SR) is the primary metric, measuring the fraction of episodes in which the autonomous system successfully navigates to the target object. An episode is considered successful if the autonomous system issues a stop action within 1 meter of the target with the target within its field of view, formally defined as $\text{SR} = \frac{1}{N}\sum_{i=1}^{N} S_i$, where N is the total number of evaluation episodes and $S_i \in \{0, 1\}$ is the binary success indicator for episode i. Success weighted by Path Length (SPL) further evaluates navigation efficiency by penalizing unnecessarily long trajectories, defined as $\text{SPL} = \frac{1}{N}\sum_{i=1}^{N} S_i \frac{l_i}{\max(p_i, l_i)}$ where l_i is the shortest possible path from the starting position to the goal and p_i is the actual path length traversed; a score closer to 1.0 indicates near-optimal path efficiency. Steps records the total number of discrete actions executed before episode termination, where a lower count reflects a more efficient search strategy. Finally, Distance to Goal (DTG) measures the geodesic distance between the autonomous system's final position and the target at episode termination, providing a continuous measure of partial progress, particularly informative for failure analysis. To evaluate system efficiency, we measure search time and token usage. Search time captures the end-to-end elapsed time from the user's

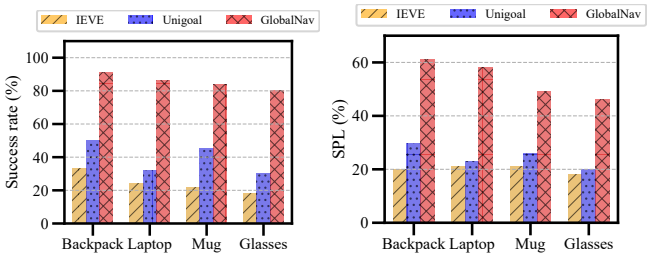

(a) Success rate (b) SPL

Figure 9: Real-world navigation performance.

Method	SR (%)↑	SPL (%)↑	DTG (m)↓	Steps↓
FreeReg [21]	17.9	15.1	10.45	438.37
IEVE [11]	53.82	33.37	4.31	293.94
UniGoal [28]	37.09	31.58	4.25	329.67
GlobalNav (Ours)	**90.91**	**51.37**	**0.78**	**150.36**

Table 2: Habitat-Simulator navigation performance.

target query to successful navigation, reflecting both navigation strategy efficiency and VLM inference latency. Token usage quantifies the total tokens consumed by VLM and LLM queries throughout an episode, serving as a direct indicator of resource efficiency.

5.2.2 Baselines. We compare GlobalNav with three representative baselines that utilize the infrastructure global view. *FreeReg* [22] registers the infrastructure image to a pre-built 3D map using cross-modality feature matching to derive navigation goals. *IEVE* [11] navigates by continuously matching a reference image of the target object against egocentric observations through visual correspondence. *UniGoal* [28] leverages VLMs to perform zero-shot navigation by extracting semantic information of the target object alongside its surrounding context, which the autonomous system matches against local observations to guide navigation. These baselines represent the current state-of-the-art across map-based, imaage matching-based, and VLM-based approaches.

5.3 An End-to-end Experiment

5.3.1 Simulator Experiments. We evaluate GlobalNav against baseline methods across various scenarios in the Habitat Simulator, with quantitative results reported in Table 2. FreeReg yields the weakest performance across all metrics. Due to the large perspective discrepancy between the elevated infrastructure camera and the ground-level autonomous system, direct projection is fundamentally unreliable, causing substantial geometric errors that mislead the autonomous system during navigation. The image matching-based method IEVE achieves a higher success rate and produces more efficient paths than the VLM-based UniGoal. This is because the

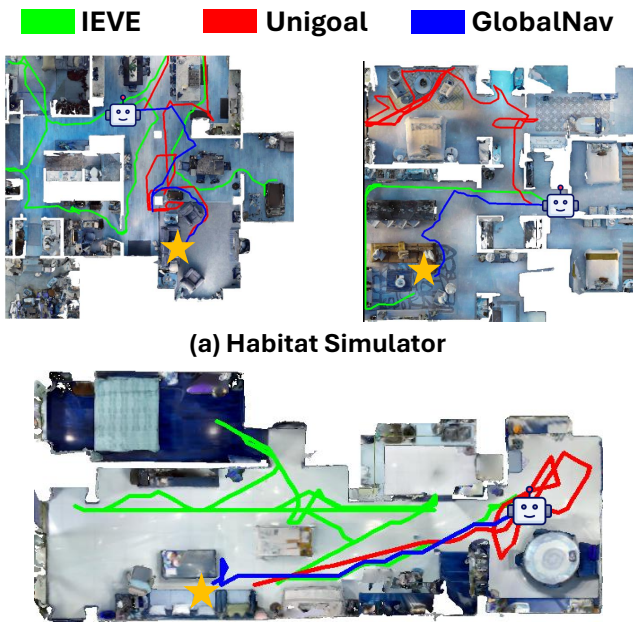

(a) Habitat Simulator

(b) Real World

Figure 10: Navigation trajectories for different methods in Habitat Simulator and Real-world setting. The yellow star indicates the location of the target object.

simulator environment is relatively simple and visually consistent, making direct image matching sufficiently reliable for landmark identification, whereas UniGoal's VLM-based reasoning is more sensitive to the limited visual diversity of synthetic scenes. Our system GlobalNav achieves approximately 40% higher success rate than the baselines while reducing navigation steps by around 50%. SPL improves by approximately 50%, indicating that GlobalNav not only reaches the target more reliably but does so via near-optimal paths, demonstrating that the hierarchical navigation strategy effectively eliminates redundant exploration. Representative trajectories of IEVE, UniGoal, and GlobalNav are visualized in Figure 10a. GlobalNav consistently produces efficient paths, whereas both IEVE and UniGoal fail to extract meaningful scene understanding from the global view, resulting in highly inefficient navigation trajectories.

5.3.2 Real-world Experiments. The real-world experimental results are presented in Figure 9, where we evaluate our system on four different target objects and compare against IEVE and UniGoal. Our system achieves approximately 85% success rate and an SPL of around 0.5, outperforming all baseline methods by over 40% and 50%, respectively, demonstrating that GlobalNav consistently reaches the target via shorter and more efficient paths. In contrast to the simulator results, UniGoal outperforms IEVE in the real-world setting. Real-world environments introduce significant visual variability,

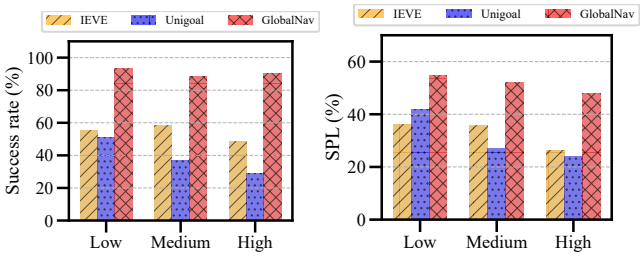

(a) Success rate (b) SPL

Figure 11: Navigation performance under different scene complexities.

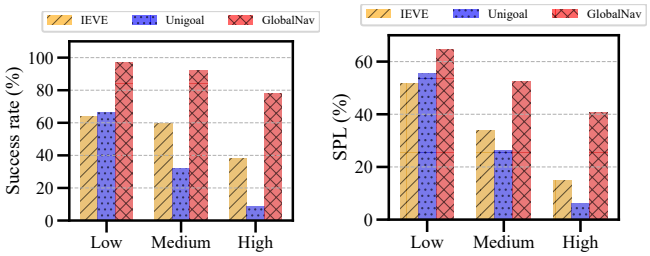

(a) Success rate (b) SPL

Figure 12: Navigation performance under different start-to-target distances

which causes image matching to produce unreliable correspondences. VLM-based reasoning, grounded in high-level semantic understanding rather than low-level appearance, is inherently more robust to such variability. Representative trajectories of all three methods are visualized in Figure 10b, further illustrating that the global view provided by the infrastructure enables fast and precise daily object navigation in real-world scenarios.

5.4 System Robustness

In this section, we evaluate GlobalNav's robustness across various conditions. We analyze the performance based on scene complexity, start-to-target distance, the number of visible landmarks, and different target categories and sizes.

5.4.1 Scene complexity. As described in Section 4.2, our collected simulator scenes span a wide range of navigational complexities, quantified by the number of navigable nodes and edges in the environment. We partition the evaluation scenes into three tiers, low, medium, and high complexity, with comparative results illustrated in Figure 11. While all baseline methods exhibit a consistent decline in performance as scene complexity increases, GlobalNav maintains stable success rates of 90% and efficiency across all three tiers. This robustness stems from GlobalNav's ability to identify salient landmarks and decompose navigation into well-defined local subgoals, regardless of scene complexity. In contrast, IEVE lacks a global route representation and becomes increasingly inefficient as the search space grows, while UniGoal struggles to comprehend complex spatial layouts from local observations alone, leading to progressively degraded performance.

5.4.2 Start-to-target distance. We further investigate how the autonomous system's initial position relative to the target object affects navigation performance. A greater starting distance increases task difficulty, as the autonomous system must navigate through more of the environment before reaching the target, encountering more decision points that accumulate errors along the way. We categorize episodes into three distance tiers: low (less than 3 m), medium (3–6 m), and high (greater than 6 m), with results shown in Figure 12. As expected, performance degrades across all methods with increasing starting distance. Notably, both IEVE and UniGoal drop to success rates below 40% and path efficiency below 20% in the high-distance tier, indicating that neither image matching nor semantic commonsense reasoning can reliably infer the location of target objects over long search horizons, leading to inefficient, wandering exploration. GlobalNav, by contrast, still achieves nearly 80% success rate in the high-distance tier. This is because it leverages the global infrastructure view to obtain spatially grounded guidance that directs the autonomous system toward the target area from the very beginning, maintaining reliable navigation performance regardless of the initial starting distance.

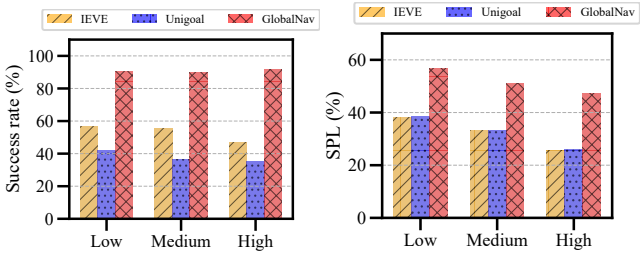

(a) Success rate (b) SPL

Figure 13: Navigation performance with different numbers of landmarks.

5.4.3 Landmark numbers. In addition, we evaluate the effect of landmark density in the infrastructure global view on navigation performance (Figure 13). A greater number of landmarks indicates a more complex environment, making it harder for the autonomous system to identify the correct target without confusion. GlobalNav maintains a high success rate of 90% across varying landmark densities, whereas both IEVE and UniGoal show a consistent drop in success rate and SPL as landmark count increases. This robustness stems from two key components: our cross-view matching algorithm ensures reliable landmark correspondence and accurate perspective alignment even in cluttered scenes, while our hierarchical navigation mechanism dynamically

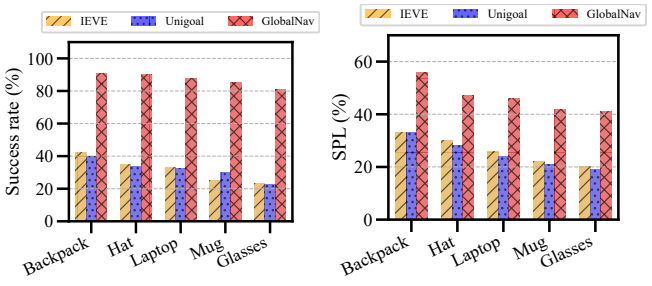

(a) Success rate (b) SPL

Figure 14: Navigation performance for different object categories.

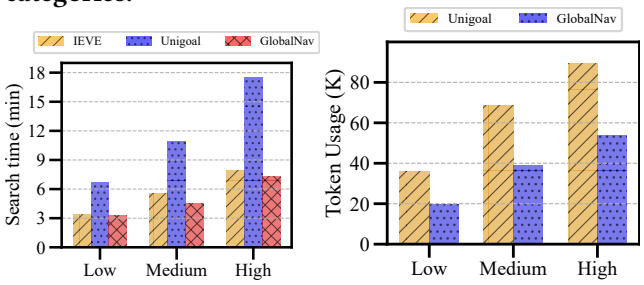

(a) Average Search time (b) Average Token usage

Figure 15: Average time and token usage under different navigation distance.

switches between landmark-level and waypoint-level guidance, preventing over-reliance on any single landmark as scene complexity grows.

5.4.4 Object categories. We evaluate GlobalNav on five target objects of varying sizes—backpack, laptop, hat, mug, and glasses—with results shown in Figure 14. GlobalNav achieves a stable success rate across objects of different sizes. SPL decreases as object size becomes smaller, since small objects can only be detected at close range, requiring more navigation steps and thus reducing path efficiency. Nevertheless, GlobalNav outperforms the baselines by approximately 50% in SPL and improves success rate by over 50% on small objects such as glasses, demonstrating that waypoint-driven navigation effectively narrows the search space and remains robust across diverse object types and scales.

5.5 System Overhead

We evaluate the end-to-end search time of GlobalNav against baseline methods in real-world settings. Search time encompasses all stages of operation, including perception, decision-making, and physical execution of the navigation route. We compare GlobalNav against IEVE and UniGoal across varying start-to-target distances, with results presented in Figure 15a. GlobalNav achieves less than half the runtime of UniGoal and requires slightly less time than IEVE, while delivering substantially better navigation performance. This efficiency stems from GlobalNav's ability to derive a more optimal route from the global infrastructure view, reducing the extent of exploratory traversal required to locate the target and thereby minimizing overall time-to-completion in real-world deployment.

Besides, we also evaluate VLM token usage of GlobalNav compared to UniGoal under different start-to-target distances, with results shown in Figure 15b. GlobalNav consumes only around 60% of the tokens used by UniGoal. This reduction is due to our hierarchical navigation strategy. In the best case, the VLM is queried only once to plan the high-level route, after which the autonomous system proceeds toward the target without further queries. Otherwise, the VLM is invoked only when a discrepancy arises between the local observation and the global view, avoiding the need for continuous querying. In contrast, UniGoal requires continuous VLM queries throughout navigation. This demonstrates that GlobalNav achieves superior navigation performance with substantially lower computational overhead.

PP	PU	WS	TC	SR(%)↑	SPL(%)↑	DTG(m)↓	Steps↓
				32.03	4.72	3.51	487.36
✓				62.24	32.23	2.53	238.47
✓	✓			65.62	36.62	2.04	218.39
✓	✓	✓		75.96	42.43	1.98	185.82
✓	✓	✓	✓	90.91	51.37	0.78	150.36

Table 3: Comparisons of stages in the navigation. PP: Path Planning. PU: Plan Update. WS: Waypoint Selection. TC: Target Confirmation.

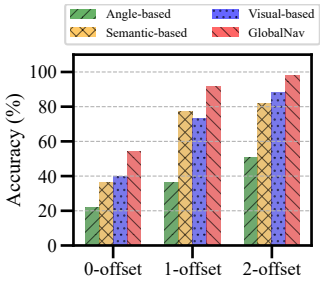

Figure 16: Accuracy of Cross-view Perspective Alignment module.

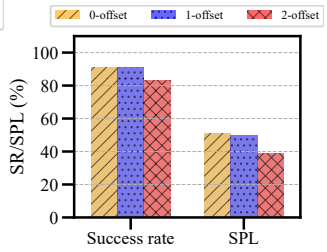

Figure 17: Impact of direction alignment errors on navigation.

5.6 Ablation Study

5.6.1 Cross-view Perspective Alignment. We evaluate our cross-view perceptive alignment module against three ablated variants: angle-only, semantic-only, and visual-only matching. Our full method combines visual appearance, semantic cues, and a discretized orientation representation that quantizes landmark-to-landmark relative orientations into 8 direction bins for robust cross-view association. As reported in Figure 16, we measure matching accuracy at three tolerance levels: 0-offset (the predicted bin exactly matches the

ground truth), and 1- and 2-offset (the prediction falls within one or two neighboring bins of the ground truth, respectively). Our approach achieves over 90% at 1-offset accuracy, outperforming the best baseline by approximately 15%.

Crucially, the VLM reasoning stage reasons over a small set of plausible direction candidates rather than requiring an exact bin prediction, such that a 1-bin error (e.g., predicting *left-front* instead of *left*) preserves the general navigational intent with negligible deviation. To confirm this, we evaluate navigation performance under three alignment conditions: ground-truth, one-bin offset, and two-bin offset (Figure 17). Results show that a one-bin offset incurs only marginal performance degradation, validating the adequacy of our matching target. In contrast, a two-bin offset leads to a nearly 10% drop in success rate and SPL, indicating that increasing perspective errors degrade navigation reliability. Together, these results demonstrate that our cross-view perceptive alignment provides sufficiently accurate correspondences to support robust downstream navigation.

5.6.2 Hiearchical stage evaluation. We evaluate our hierarchical navigation decision mechanism through a staged ablation study, where each component is incrementally added to isolate its individual contribution, with results presented in Table 3. The baseline condition corresponds to the autonomous system performing a blind search without any infrastructure guidance. Incorporating global-view landmark guidance yields a substantial improvement in success rate of 30%, demonstrating that landmarks provide effective high-level guidance for directing the autonomous system toward the target. Further incorporating waypoint selection and target confirmation introduces additional performance gains of 10% and 15%, respectively, indicating that landmark guidance alone is insufficient for reliable navigation. The waypoint-driven navigation bridges the viewpoint discrepancy between the autonomous system's local egocentric observations and the infrastructure's global view, enabling more reliable correspondence and consistent navigation guidance. These results confirm that each component of the hierarchical mechanism contributes meaningfully to the overall robustness of the system.

6 RELATED WORK

Object Goal Navigation Object goal navigation (ObjectNav) requires an autonomous system to locate a target object in an unexplored environment. Early methods train end-to-end policies from large-scale simulation data [5, 13, 31], but generalize poorly to real-world settings. To improve generalization, LLM and VLM-based methods leverage commonsense reasoning to guide exploration [33, 12, 6], while others build persistent semantic maps or scene graphs [32, 30, 23] to encode spatial context. However, daily objects are inherently dynamic, making commonsense priors unreliable and static maps unable to reflect their current locations. GlobalNav overcomes these limitations by getting navigation decisions from the infrastructure's global view, enabling reliable retrieval of arbitrarily placed daily objects.

Instance Image Goal Navigation Instance image goal navigation (InstanceImageNav)[10, 11, 19] requires the autonomous system to locate a specific object instance through cross-view image matching. More recently, VLM-based methods[28, 14] encode the reference image alongside its semantic context into a rich embedding, which the autonomous system continuously matches against egocentric observations to guide navigation. However, these methods focus narrowly on matching the target object's appearance and assume the reference image shares a similar viewpoint with the robot, making them unreliable when the reference comes from an elevated infrastructure camera. They also lack the ability to leverage the rich scene-level context that the global view provides for navigation. GlobalNav directly addresses both limitations by aligning cross-view perspectives and exploiting global scene context for informed navigation guidance.

7 DISCUSSION

Multiple infrastructure cameras. Our system assumes that the target object is visible within a single infrastructure camera and uses that camera to guide the autonomous system throughout navigation. In practice, large environments such as commercial centers or multi-room buildings may require multiple cameras with overlapping or non-overlapping coverage zones. Extending GlobalNav to support multi-camera coordination and seamless handoff between cameras would be a promising direction for future large-scale deployments.
Outdoor scenario. GlobalNav is designed for indoor autonomous systems to assist users in retrieving daily objects. This paradigm can be naturally extended to outdoor settings, such as delivery autonomous systems operating across open streetscapes, where roadside cameras could provide a similar global view to guide navigation. We leave this direction as a future work.

8 CONCLUSION

In this paper, we introduce GlobalNav, the first VLM-based navigation system that leverages the global view from widely deployed infrastructure cameras to guide autonomous systems in locating daily movable objects. By integrating infrastructure global view with the autonomous system's local view, GlobalNav enables reliable navigation toward arbitrarily placed daily objects without relying on pre-built maps or commonsense priors. Extensive experiments demonstrate that GlobalNav achieves a significantly higher success rate, more efficient navigation paths, and reduced search time compared to state-of-the-art baselines.

REFERENCES

[1] Peter Anderson, Qi Wu, Damien Teney, Jake Bruce, Mark Johnson, Niko Sünderhauf, Ian Reid, Stephen Gould, and Anton Van Den Hengel. 2018. Vision-and-language navigation: interpreting visually-grounded navigation instructions in real environments. In *Proceedings of the IEEE conference on computer vision and pattern recognition*, 3674–3683.

[2] Luca Barsellotti, Roberto Bigazzi, Marcella Cornia, Lorenzo Baraldi, and Rita Cucchiara. 2024. Personalized instance-based navigation toward user-specific objects in realistic environments. *Advances in Neural Information Processing Systems*, 37, 11228–11250.

[3] Aleksei Bochkovskii, Amaël Delaunoy, Hugo Germain, Marcel Santos, Yichao Zhou, Stephan R. Richter, and Vladlen Koltun. 2025. Depth pro: sharp monocular metric depth in less than a second. In *International Conference on Learning Representations*. https://arxiv.org/abs/2410.02073.

[4] Bach-Thuan Bui, Huy-Hoang Bui, Dinh-Tuan Tran, and Joo-Ho Lee. 2024. Representing 3d sparse map points and lines for camera relocalization.

[5] Devendra Singh Chaplot, Dhiraj Prakashchand Gandhi, Abhinav Gupta, and Russ R Salakhutdinov. 2020. Object goal navigation using goal-oriented semantic exploration. *Advances in Neural Information Processing Systems*, 33, 4247–4258.

[6] Junting Chen, Guohao Li, Suryansh Kumar, Bernard Ghanem, and Fisher Yu. 2023. How to not train your dragon: training-free embodied object goal navigation with semantic frontiers. *arXiv preprint arXiv:2305.16925*.

[7] Zhou Fan, Cheng Mao, Yihong Wu, and Jiaming Xu. 2020. Spectral graph matching and regularized quadratic relaxations: algorithm and theory. In *Proceedings of the 37th International Conference on Machine Learning* (Proceedings of Machine Learning Research). Hal Daumé III and Aarti Singh, (Eds.) Vol. 119. PMLR, (13–18 Jul 2020), 2985–2995. https://proceedings.mlr.press/v119/fan20a.html.

[8] International Federation of Robotics. 2024. Sales of service robots up 30% worldwide. https://ifr.org/ifr-press-releases/news/sales-of-service-robots-up-30-worldwide. World Robotics 2024 Service Robots Report. Accessed: 2025. (Oct. 2024).

[9] Nidhi Kalra, Dave Ferguson, and Anthony Stentz. 2009. Incremental reconstruction of generalized voronoi diagrams on grids. *Robotics and Autonomous Systems*, 57, 2, 123–128.

[10] Jacob Krantz, Stefan Lee, Jitendra Malik, Dhruv Batra, and Devendra Singh Chaplot. 2022. Instance-specific image goal navigation: training embodied agents to find object instances. *arXiv preprint arXiv:2211.15876*.

[11] Xiaohan Lei, Min Wang, Wengang Zhou, Li Li, and Houqiang Li. 2024. Instance-aware exploration-verification-exploitation for instance imagegoal navigation. In *Proceedings of the IEEE/CVF Conference on Computer Vision and Pattern Recognition*, 16329–16339.

[12] Yuxing Long, Wenzhe Cai, Hongcheng Wang, Guanqi Zhan, and Hao Dong. 2024. Instructnav: zero-shot system for generic instruction navigation in unexplored environment. *arXiv preprint arXiv:2406.04882*.

[13] Arjun Majumdar, Gunjan Aggarwal, Bhavika Devnani, Judy Hoffman, and Dhruv Batra. 2022. Zson: zero-shot object-goal navigation using multimodal goal embeddings. *Advances in Neural Information Processing Systems*, 35, 32340–32352.

[14] Dujun Nie, Xianda Guo, Yiqun Duan, Ruijun Zhang, and Long Chen. 2025. Wmnav: integrating vision-language models into world models for object goal navigation. In *2025 IEEE/RSJ International Conference on Intelligent Robots and Systems (IROS)*. IEEE, 2392–2399.

[15] [n. d.] Polycam. https://poly.cam/. 3D scanning and photogrammetry software (accessed 2026-03-14). ().

[16] Xavi Puig et al. 2023. Habitat 3.0: a co-habitat for humans, avatars and robots. (2023).

[17] Santhosh Kumar Ramakrishnan et al. 2021. Habitat-matterport 3d dataset (HM3d): 1000 large-scale 3d environments for embodied AI. In *Thirty-fifth Conference on Neural Information Processing Systems Datasets and Benchmarks Track*. https://arxiv.org/abs/2109.08238.

[18] Tianhe Ren et al. 2024. Grounded sam: assembling open-world models for diverse visual tasks. *ArXiv*, abs/2401.14159. https://api.semanticscholar.org/CorpusID:267212047.

[19] Xinyu Sun, Peihao Chen, Jugang Fan, Jian Chen, Thomas Li, and Mingkui Tan. [n. d.] Fgprompt: fine-grained goal prompting for image-goal navigation. *Advances in Neural Information Processing Systems*, 36.

[20] SAM 3D Team et al. 2025. Sam 3d: 3dfy anything in images. https://arxiv.org/abs/2511.16624 arXiv: 2511.16624 [cs.CV].

[21] Anirudh Topiwala, Pranav Inani, and Abhishek Kathpal. 2018. Frontier based exploration for autonomous robot. *ArXiv*, abs/1806.03581. https://api.semanticscholar.org/CorpusID:47017346.

[22] Haiping Wang, Yuan Liu, Bing Wang, Yujing Sun, Zhen Dong, Wenping Wang, and Bisheng Yang. 2023. Freereg: image-to-point cloud registration leveraging pretrained diffusion models and monocular depth estimators. *arXiv preprint arXiv:2310.03420*.

[23] Neng Wang, Huimin Lu, Zhiqiang Zheng, Hesheng Wang, Yun-Hui Liu, and Xieyuanli Chen. 2025. Leveraging semantic graphs for efficient and robust lidar slam. *2025 IEEE/RSJ International Conference on Intelligent Robots and Systems (IROS)*, 1614–1621. https://api.semanticscholar.org/CorpusID:277043800.

[24] Pengying Wu, Yao Mu, Bingxian Wu, Yi Hou, Ji Ma, Shanghang Zhang, and Chang Liu. 2024. Voronav: voronoi-based zero-shot object navigation with large language model. *arXiv preprint arXiv:2401.02695*.

[25] Chunyu Xie, Bin Wang, Fanjing Kong, Jincheng Li, Dawei Liang, Gengshen Zhang, Dawei Leng, and Yuhui Yin. 2025. Fg-clip: fine-grained visual and textual alignment. *arXiv preprint arXiv:2505.05071*.

[26] Shuo Xing, Zezhou Sun, Shuangyu Xie, Kaiyuan Chen, Yanjia Huang, Yuping Wang, Jiachen Li, Dezhen Song, and Zhengzhong Tu. 2025. Can large vision language models read maps like a human? *arXiv preprint arXiv:2503.14607*.

[27] Hang Yin, Xiuwei Xu, Zhenyu Wu, Jie Zhou, and Jiwen Lu. 2024. Sg-nav: online 3d scene graph prompting for llm-based zero-shot object navigation. *ArXiv*, abs/2410.08189. https://api.semanticscholar.org/CorpusID:273233851.

[28] Hang Yin, Xiuwei Xu, Linqing Zhao, Ziwei Wang, Jie Zhou, and Jiwen Lu. 2025. Unigoal: towards universal zero-shot goal-oriented navigation. In *Proceedings of the IEEE/CVF Conference on Computer Vision and Pattern Recognition*, 19057–19066.

[29] Bangguo Yu, Hamidreza Kasaei, and Ming Cao. 2023. Frontier semantic exploration for visual target navigation. *2023 IEEE International Conference on Robotics and Automation (ICRA)*, 4099–4105. https://api.semanticscholar.org/CorpusID:258078886.

[30] Tatiana Zemskova and Dmitry A. Yudin. 2024. 3dgraphllm: combining semantic graphs and large language models for 3d scene understanding. *ArXiv*, abs/2412.18450. https://api.semanticscholar.org/CorpusID:274992199.

[31] Jiazhao Zhang, Liu Dai, Fanpeng Meng, Qingnan Fan, Xuelin Chen, Kai Xu, and He Wang. 2023. 3d-aware object goal navigation via simultaneous exploration and identification. In *Proceedings of the IEEE/CVF Conference on Computer Vision and Pattern Recognition*, 6672–6682.

[32] Lingfeng Zhang et al. 2025. Mapnav: a novel memory representation via annotated semantic maps for vlm-based vision-and-language navigation. *ArXiv*, abs/2502.13451. https://api.semanticscholar.org/CorpusID:276449634.

[33] Gengze Zhou, Yicong Hong, and Qi Wu. 2024. Navgpt: explicit reasoning in vision-and-language navigation with large language models. In *Proceedings of the AAAI Conference on Artificial Intelligence* number 7. Vol. 38, 7641–7649.